Hydrogenation of edible oils and fats

Jonker, Geert Hilbertus

3. Diene kinetics [*]

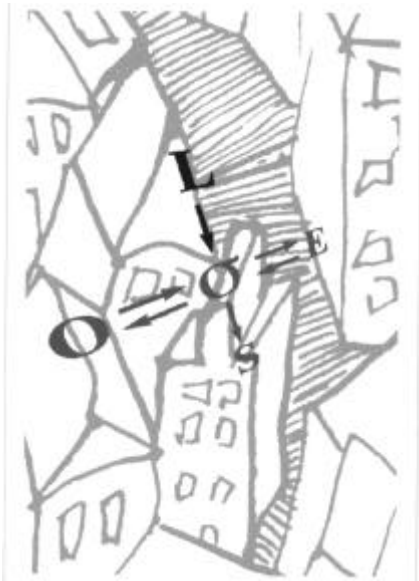

Under industrial conditions, 373 < T < 473 K and 0.1 < P_{H_2} < 1.0 MPa, poly unsaturated fatty acids are hydrogenated preferentially over the mono unsaturated species. But many side products are produced too, which frustrates the construction of a realistic reaction rate equation. However, based on the selected rate determining steps, obtained for the monoene kinetics (chapter 2), we have developed rate equations for the diene hydrogenation and cis–trans isomerization with one new parameter only. This chapter reports on the development of the monoene-based diene reaction mechanism and on experiments to verify the obtained rate equations.

[*] Submitted to *Ind. Chem. Eng. Res.* as "An Intrinsic kinetic model for the hydrogenation of double unsaturated fatty acid methyl esters over nickel-based catalysts based on the Horiuty–Polanyi mechanism"; Bouma, M. J.; Jonker, G. H.; Veldsink, J. W.; Beenackers, A. A. C. M.

3.1. Introduction

A vast amount of studies has been assigned to the kinetics of hydrogenation of polyunsaturated fats, aiming at selectivity improvement (Veldsink et al., 1997). However, simultaneous migration and *cis-trans* isomerization during the hydrogenation hampered the establishment of intrinsic rate equations. Therefore, early rate equations for the hydrogenation of the double unsaturated fatty acid Linoleate (diene), were merely based on the degree of unsaturation: Linoleate→Oleate→Stearate and presented as first order or power law kinetics.

Applying the Horiuti-Polanyi mechanism Hashimoto et al. (1971), Gut et al (1979) and Grau et al. (1987a,b) incorporated *cis-trans* isomerization in the monounsaturated compounds (monoenes) according to the scheme in Figure 3.1. Hashimoto et al. (1971) derived the rate equations as overall first order kinetics, thus omitting possible saturation of the active catalyst sites with reactants. Gut et al. (1979) applied Langmuir–Hinshelwood type adsorption of unsaturates on the active sites and were able to describe the initial zero-order behavior of the diene. Rate constants as well as adsorption constants were reported. Limited by the applied calculation method, Grau et al (1987a,b) were able to determine lumped rate and adsorption constants only.

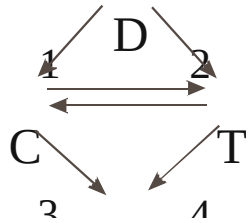

Figure 3.1. Diene hydrogenation scheme used by Hashimoto et al. (1971), Gut et al. (1979) and Grau et al (1987). D, diene; C, *cis* monoene; T, *trans* monoene; S, saturated.

However, overall schemes, such as in Figure 3.1, neglect isomerization within the level of dienes and lump mechanistic steps into overall routes. For instance, if linoleic acid or its methyl ester (*cis*,*cis*) diene is hydrogenated, the direct route to *trans* monoene, denoted route 2 in Figure 3.1, has no mechanistic meaning. In terms of the Horiuti–Polanyi mechanism it combines a hydrogenation and an isomerization step. Though the rate equations derived from such a scheme may satisfactorily predict hydrogenation and isomerization rates under the conditions applied, extrapolation to the hydrogenation of diene *cis-trans* isomers will fail. While direct hydrogenation of a diene (L) with increased *trans* content will yield higher *trans* monoene in practice, it has no influence on the ratio of the rates of route 1 and 2 in the model.

Usually, different adsorption strengths of fatty acids on the catalyst surface are mentioned as the explanation for the difference in reaction rates of different types of unsaturated methyl esters (Eldib and Albright, 1957; Albright, 1963; Coenen and Boerma, 1968; Heertje and Boerma, 1971; Albright, 1985; Babenkova et al. 1994). For instance, Coenen and Boerma (1968) observed zero-order behavior with respect to the unsaturated compound in the hydrogenation of safflower oil and explained it by complete catalyst surface occupancy of linoleic methyl ester, due to strong adsorption relative to the monoene. In the hydrogenation of a mixture of linoleic acid and labeled oleic acid, Coenen and Boerma (1968) and Heertje and Boerma (1971) found that none of the initially formed elaidate and stearate was labeled. From this, they concluded that unlabeled elaidic acid and stearic acid were formed directly from linoleic acid, and, if linoleic acid was present, hardly any of the monoenic acid in the liquid bulk could adsorb on the catalyst surface.

The aim of this chapter is to extend the rate equations for the hydrogenation of monoenes to the hydrogenation and isomerization of dienes. Here, it will be tested whether the same (Horiuti–Polanyi) reaction mechanism that proved successful in describing the monoene hydrogenation (chapter 2) is applicable to the diene hydrogenation reactions as well. The selected rate equations were:

$$R_{\mathrm{O}} = m_{\mathrm{c}} \frac{-(k \ + k_2 K_{\mathrm{iso}}) C_{\mathrm{O}} + k_2 C_{\mathrm{E}}}{C_{\mathrm{O}} + C_{\mathrm{E}} + k_4 C_{\mathrm{S}}} K_{\mathrm{H}} P_{\mathrm{H_2}} \tag{3.1}$$

$$R_{\mathrm{E}} = m_{\mathrm{c}} \frac{-(k_3 + k_2) C_{\mathrm{E}} + k_2 K_{\mathrm{iso}} C_{\mathrm{O}}}{C_{\mathrm{O}} + C_{\mathrm{E}} + k_4 C_{\mathrm{S}}} K_{\mathrm{H}} P_{\mathrm{H_2}} \tag{3.2}$$

This approach yields a repetitive scheme of hydrogenation and isomerization where the kinetic rate constants are taken from the monoenic kinetic study of chapter 2 and where the adsoption constant of dienes, K_{D}, remains the only new parameter to be determined experimentally. The resulting rate equations are tested on a set of batch linoleate hydrogenation experiments with varying temperature and hydrogen pressure.

3.2. Theory

An extension of the monoene hydrogenation mechanism of chapter 2 can be obtained by assuming that the hydrogenation of double bonds of dienes can be described by the same rate equations expressed in surface concentrations as proved to be valid for monoene hydrogenation. In this model the observed greater reactivity of the dienes stems from the strong adsorption of dienes relative to monoenes only. The latter is generally accepted from indirect evidence in hydrogenation experiments (Albright, 1963; Coenen and Boerma, 1971; Susu et al., 1978; Babenkova et al., 1994). The reaction scheme is depicted in Figure 3.2. If it is assumed that the non-attacked double bond in the half-hydrogenated diene intermediate exerts no influence on the reaction steps, the adsorbed diene can be considered as a strongly adsorbed monoene.

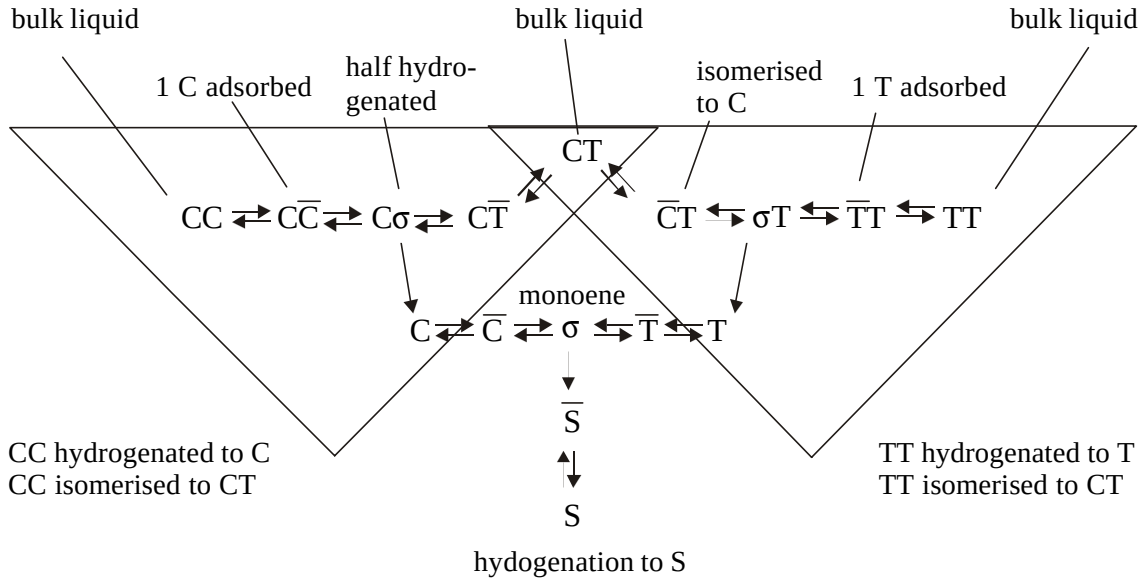

Figure 3.2. Reaction mechanism of diene hydrogenation.

The elementary reaction steps of such a single adsorbed diene are then the same as for monoenes. Both hydrogenation and isomerization proceed via the half-hydrogenated state and in each reaction path the insertion of hydrogen in the adsorbed double bond is the rate-determining step.

Equivalents of the monoene hydrogenation triangle (C-T-S, see also Figure 3.1) appear twice at the diene level of the mechanism (CC-CT-C and CT-CC-T, Figure

3.2). For example, the $\overline{C}T$ diene, adsorbed with the *cis* double bond, reacts towards the Cσ-complex in the same way as $\overline{C}$ forms the σ-complex. The individual reaction steps and accompanying rate or equilibrium equations of the diene reaction scheme, including the monoene reactions are given in Table 3.1.

For the establishment of rate equations, the following assumptions are applied, following the methodology of chapter 2

(1) Noncompetitive adsorption of hydrogen and the fatty acids.

(2) Fatty acids adsorption, reactions 1-7 in Table 3.1, is at equilibrium.

(3) Hydrogen adsorption, reaction 8 in Table 3.1, is at equilibrium,

(4) The surface fractions of the σ-intermediates as depicted in Figure 3.2 are negligible, due to their high reactivity. With assumption 1 it then follows:

$$q_{\overline{C}C} + q_{\overline{C}T} + q_{C\overline{T}} + q_{\overline{T}T} + q_{\overline{C}} + q_{\overline{T}} + q_{\overline{S}} + q_V \approx 1 \qquad (3.3)$$

(5) The active sites for fatty acids are occupied completely,

$$q_{\overline{C}C} + q_{\overline{C}T} + q_{C\overline{T}} + q_{\overline{T}T} + q_{\overline{C}} + q_{\overline{T}} + q_{\overline{S}} >> q_V \qquad (3.4)$$

(6) The adsorption constants for *cis* and *trans* double bonds in the monoenes and the dienes are equal

$$K_{\overline{C}} = K_{\overline{T}} = K_{\overline{M}} \qquad (3.5)$$

$$K_{\overline{C}C} = K_{\overline{C}T} = K_{C\overline{T}} = K_{\overline{T}T} = K_{\overline{D}} \qquad (3.6)$$

(7) The rate constants for the formation of the σ-complex from *cis*, respectively, *trans* double bonds, are independent of the degree of unsaturation. Hence:

$$k_{f,\overline{C}C} = k_{f,\overline{C}T} = k_{f,C}$$

$$k_{b,\overline{C}C} = k_{b,\overline{C}T} = k_{b,\overline{C}}$$

$$k_{f,\overline{T}T} = k_{f,C\overline{T}} = k_{f,\overline{T}}$$

$$k_{b,\overline{T}T} = k_{b,C\overline{T}} = k_{b,\overline{T}}$$

$$K_{I,\overline{C}C} = K_{I,\overline{C}T} = K_{I,\overline{C}}$$

$$K_{I,\overline{T}T} = K_{I,C\overline{T}} = K_{I,\overline{T}} \qquad (3.7)$$

(8) The location of the double bonds has no influence on reaction rates.

(9) The rate and adsorption constants follow an Arrhenius type of temperature dependence:

Table 3.1. Elementary Reaction Steps, Rate Equations and Equilibrium Constants in the Diene Hydrogenation Model.

j	reaction eq	R_{ES}/m_c	equilibrium constant
1	$CC+V \underset{k_{d,\bar{C}C}}{\overset{k_{a,\bar{C}C}}{\rightleftharpoons}} \bar{C}C$	$k_{a,\bar{C}C}C_{CC}\theta_V - k_{d,\bar{C}C}\theta_{\bar{C}C}$	$K_{\bar{C}C}=\frac{k_{a,\bar{C}C}}{k_{d,\bar{C}C}}=\frac{\theta_{\bar{C}C}}{C_{CC}\theta_V}$
2	$CT+V \underset{k_{d,\bar{C}T}}{\overset{k_{a,\bar{C}T}}{\rightleftharpoons}} \bar{C}T$	$k_{a,\bar{C}T}C_{CT}\theta_V - k_{d,\bar{C}T}\theta_{\bar{C}T}$	$K_{\bar{C}T}=\frac{k_{a,\bar{C}T}}{k_{d,\bar{C}T}}=\frac{\theta_{\bar{C}T}}{C_{CT}\theta_V}$
3	$CT+V \underset{k_{d,C\bar{T}}}{\overset{k_{a,C\bar{T}}}{\rightleftharpoons}} C\bar{T}$	$k_{a,C\bar{T}}C_{CT}\theta_V - k_{d,C\bar{T}}\theta_{C\bar{T}}$	$K_{C\bar{T}}=\frac{k_{a,C\bar{T}}}{k_{d,C\bar{T}}}=\frac{\theta_{C\bar{T}}}{C_{CT}\theta_V}$
4	$TT+V \underset{k_{d,\bar{T}T}}{\overset{k_{a,\bar{T}T}}{\rightleftharpoons}} \bar{T}T$	$k_{a,\bar{T}T}C_{TT}\theta_V - k_{d,\bar{T}T}\theta_{\bar{T}T}$	$K_{\bar{T}T}=\frac{k_{a,\bar{T}T}}{k_{d,\bar{T}T}}=\frac{\theta_{\bar{T}T}}{C_{TT}\theta_V}$
5	$C+V \underset{k_{d,\bar{C}}}{\overset{k_{a,\bar{C}}}{\rightleftharpoons}} \bar{C}$	$k_{a,\bar{C}}C_C\theta_V - k_{d,\bar{C}}\theta_{\bar{C}}$	$K_{\bar{C}}=\frac{k_{a,\bar{C}}}{k_{d,\bar{C}}}=\frac{\theta_{\bar{C}}}{C_C\theta_V}$
6	$T+V \underset{k_{d,\bar{T}}}{\overset{k_{a,\bar{T}}}{\rightleftharpoons}} \bar{T}$	$k_{a,T}C_T\theta_V - k_{d,T}\theta_T$	$K_{\bar{T}}=\frac{k_{a,\bar{T}}}{k_{d,\bar{T}}}=\frac{\theta_{\bar{T}}}{C_T\theta_V}$
7	$S+V \underset{k_{d,\bar{S}}}{\overset{k_{a,\bar{S}}}{\rightleftharpoons}} \bar{S}$	$k_{a,\bar{S}}C_S\theta_V - k_{d,\bar{S}}\theta_{\bar{S}}$	$K_{\bar{S}}=\frac{k_{a,\bar{S}}}{k_{d,\bar{S}}}=\frac{\theta_{\bar{S}}}{C_S\theta_V}$
8	$H_2+V_H \underset{k_{d,\bar{H}2}}{\overset{k_{a,\bar{H}2}}{\rightleftharpoons}} \bar{H}_2$		$K_{\bar{H}2}=\frac{k_{a,\bar{H}2}}{k_{d,\bar{H}2}}=\frac{\theta_{\bar{H}2}}{P_{H_2}\theta_V}$
9	$\bar{C}C+\bar{H} \underset{k_{b,\bar{C}C}}{\overset{k_{f,\bar{C}C}}{\rightleftharpoons}} \sigma C+V_H$	$k_{f,CC}\theta_{CC}\theta_H - k_{b,CC}\theta_{\sigma C}\theta_{VH}$	$K_{I,\bar{C}C}=\frac{k_{f,\bar{C}C}}{k_{b,\bar{C}C}}=\frac{\theta_{\sigma C}\theta_{VH}}{\theta_{\bar{C}C}\theta_{\bar{H}}}$
10	$\bar{C}T+\bar{H} \underset{k_{b,\bar{C}T}}{\overset{k_{f,\bar{C}T}}{\rightleftharpoons}} \sigma T+V_H$	$k_{f,\bar{C}T}\theta_{\bar{C}T}\theta_{\bar{H}} - k_{b,\bar{C}T}\theta_{\sigma T}\theta_{VH}$	$K_{I,\bar{C}T}=\frac{k_{f,\bar{C}T}}{k_{b,\bar{C}T}}=\frac{\theta_{\sigma T}\theta_{V_H}}{\theta_{\bar{C}T}\theta_{\bar{H}}}$
11	$C\bar{T}+\bar{H} \underset{k_{b,C\bar{T}}}{\overset{k_{f,C\bar{T}}}{\rightleftharpoons}} C\sigma+V_H$	$k_{f,C\bar{T}}\theta_{C\bar{T}}\theta_{\bar{H}} - k_{b,C\bar{T}}\theta_{C\sigma}\theta_{VH}$	$K_{I,C\bar{T}}=\frac{k_{f,C\bar{T}}}{k_{b,C\bar{T}}}=\frac{\theta_{C\sigma}\theta_{V_H}}{\theta_{C\bar{T}}\theta_{\bar{H}}}$
12	$\bar{T}T+\bar{H} \underset{k_{b,\bar{T}T}}{\overset{k_{f,\bar{T}T}}{\rightleftharpoons}} \sigma T+V_H$	$k_{f,\bar{T}T}\theta_{\bar{T}T}\theta_{\bar{H}} - k_{b,\bar{T}T}\theta_{\sigma T}\theta_{VH}$	$K_{I,\bar{T}T}=\frac{k_{f,\bar{T}T}}{k_{b,\bar{T}T}}=\frac{\theta_{\sigma T}\theta_{V_H}}{\theta_{TT}\theta_H}$
13	$C+H \underset{k_{b,\bar{C}}}{\overset{k_{f,\bar{C}}}{\rightleftharpoons}} \sigma+V_H$	$k_{f,\bar{C}}\theta_{\bar{C}}\theta_{\bar{H}} - k_{b,\bar{C}}\theta_\sigma\theta_{VH}$	$K_{I,\bar{C}}=\frac{k_{f,\bar{C}}}{k_{b,\bar{C}}}=\frac{\theta_\sigma\theta_{V_H}}{\theta_C\theta_H}$
14	$\bar{T}+\bar{H} \underset{k_{b,\bar{T}}}{\overset{k_{f,\bar{T}}}{\rightleftharpoons}} \sigma+V_H$	$k_{f,\bar{T}}\theta_{\bar{T}}\theta_{\bar{H}} - k_{b,\bar{T}}\theta_\sigma\theta_{VH}$	$K_{I,\bar{T}}=\frac{k_{f,\bar{T}}}{k_{b,\bar{T}}}=\frac{\theta_\sigma\theta_{V_H}}{\theta_{\bar{T}}\theta_{\bar{H}}}$
15	$C\sigma+\bar{H} \xrightarrow{k_h} C+V_H$	$k_h\theta_{C\sigma}\theta_{\bar{H}}$	
16	$\sigma T+\bar{H} \xrightarrow{k_h} T+V_H$	$k_h\theta_{\sigma T}\theta_{\bar{H}}$	
17	$\sigma+\bar{H} \xrightarrow{k_h} \bar{S}+V_H$	$k_h\theta_\sigma\theta_{\bar{H}}$	

$$k_i(T) = k_{i,\mathrm{ref}} \exp\left(\frac{-E_{\mathrm{a},i}}{R_{\mathrm{gas}} T_{\mathrm{ref}}} \frac{T_{\mathrm{ref}} - T}{T} \right) \tag{3.8}$$

As a consequence of assumption 8, there is no distinction between double bonds at the original 9 and 12 positions in the diene. For example, the compounds C_9T_{12} and T_9C_{12} are denoted as compound CT in the model. The same holds for the monoenes produced from the dienes: C_9 and C_{12} are taken as C. The CT-diene has two possible adsorption states, each yielding different reaction products. Isomerization of, for instance, the C-adsorbed $\overline{\mathrm{C}}\mathrm{T}$-diene can only result in TT-diene, whereas hydrogenation yields T-monoene.

The thermodynamic *trans-cis* equilibrium, introduced in chapter 2 (eq 2.1) gives, following assumptions 6 and 7

$$K_{\mathrm{iso}} = \frac{K_{\overline{\mathrm{C}}\mathrm{C}} K_{\mathrm{I},\overline{\mathrm{C}}\mathrm{C}}}{K_{\mathrm{C}\overline{\mathrm{T}}} K_{\mathrm{I},\mathrm{C}\overline{\mathrm{T}}}} = \frac{K_{\overline{\mathrm{C}}\mathrm{T}} K_{\mathrm{I},\overline{\mathrm{C}}\mathrm{T}}}{K_{\mathrm{TT}} K_{\mathrm{I},\mathrm{TT}}} \tag{3.9}$$

Furthermore, from the definitions of the adsorption equilibrium constants in Table 3.1 and assumption 6, equal surface occupancies of $\mathrm{C}\overline{\mathrm{T}}$ and $\overline{\mathrm{C}}\mathrm{T}$ follow:

$$q_{\overline{\mathrm{C}\overline{\mathrm{T}}}} = q_{\mathrm{C}\overline{\mathrm{T}}} + q_{\overline{\mathrm{C}}\mathrm{T}} \tag{3.10}$$

$$q_{\overline{\mathrm{C}}\mathrm{T}} = q_{\mathrm{C}\overline{\mathrm{T}}} = \tfrac{1}{2} q_{\overline{\mathrm{C}\overline{\mathrm{T}}}} \tag{3.11}$$

Using the total adsorbed *cis-trans* diene $\overline{\mathrm{C}\overline{\mathrm{T}}}$, eq 3.11 can be substituted in the equations of Table 3.1.

The surface site balance for hydrogen is

$$q_{\mathrm{V_H}} + q_{\overline{\mathrm{H}}} = 1 \tag{3.12}$$

Substitution of $q_{\mathrm{V_H}}$ from eq 3.12 in the equation for associative hydrogen adsorption, eq 8 in Table 3.1, results in the surface fraction of hydrogen, which is equal to eq 2.10, obtained from monoene kinetics

$$q_{\mathrm{H}} = \frac{K_{\mathrm{H}} P_{\mathrm{H_2}}}{1 + K_{\mathrm{H}} P_{\mathrm{H_2}}} \tag{3.13}$$

An explicit equation for q_V is obtained upon substitution of the adsorption equilibria, eqs 1-7 of Table 3.1, in the surface sites balance for the fatty compounds, eq 3.3, and subsequently applying assumption 4:

$$q_V = (K_{\overline{S}} C_S + K_{\overline{C}} C_C + K_{\overline{T}} C_T + K_{\overline{CC}} C_{CC} + K_{\overline{CT}} C_{CT} + K_{\overline{TT}} C_{\overline{TT}})^{-1} \qquad (3.15)$$

Following chapter 2, the overall rate equations for the bulk components are evaluated in terms of independent, isomerization and hydrogenation paths

$$R_i = R_i^{iso} + R_i^{h} \qquad i\text{=CC, CT, TT, C, T} \qquad (3.16)$$

In the hydrogenation as well as the isomerization paths, the first hydrogen insertions are the rate-determining steps, as follows from the results of chapter 2. Because the hydrogenation paths, R_i^h, are irreversible, R_i^h contains the left hand term of rate equations 9–14 of Table 3.1 only. For the reversible isomerization pathways, the terms $q_{Cs} q_{V_H}$, $q_{qT} q_{V_H}$, and $q_s q_{V_H}$ are eliminated from eqs 9–14 of Table 3.1, by assuming the intermediates to be in pseudo steady state. Table 3.2 gives the final rate equations, expressed in bulk concentrations.

Table 3.2. Diene Model Rate Equations for the Bulk Components [a]

cp.	rate equation R_i/m_c
CC	$\left(-(k_1 + k_2 K_{iso}) \tilde{K}_{\overline{D}} C_{CC} + k_2 \tilde{K}_{\overline{D}} \frac{1}{2} C_{CT}\right) q_{\overline{H}} q_V$
CT	$\left(k_2 K_{iso} \tilde{K}_{\overline{D}} C_{CC} + k_2 \tilde{K}_{\overline{D}} C_{TT} - (k_3 + k_2 + k_1 + k_2 K_{iso}) \tilde{K}_{\overline{D}} \frac{1}{2} C_{CT}\right) q_{\overline{H}} q_V$
TT	$\left(-(k_3 + k_2) \tilde{K}_{\overline{D}} C_{TT} + k_2 K_{iso} \tilde{K}_{\overline{D}} \frac{1}{2} C_{CT}\right) q_{\overline{H}} q_V$
C	$\left(k_1 \tilde{K}_{\overline{D}} C_{CC} + k_3 \tilde{K}_{\overline{D}} \frac{1}{2} C_{CT} - (k_1 + k_2 K_{iso}) \tilde{K}_{\overline{M}} C_C + k_2 \tilde{K}_{\overline{M}} C_T\right) q_{\overline{H}} q_V$
T	$\left(k_1 \tilde{K}_{\overline{D}} \frac{1}{2} C_{CT} + k_3 \tilde{K}_{\overline{D}} C_{TT} + k_2 K_{iso} \tilde{K}_{\overline{M}} C_C - (k_2 + k_3) \tilde{K}_{\overline{M}} C_T\right) q_{\overline{H}} q_V$
S	$\left(k_1 \tilde{K}_{\overline{M}} C_C + k_3 \tilde{K}_{\overline{M}} C_T\right) q_{\overline{H}} q_V$

[a] $q_V = \left(C_S + \tilde{K}_{\overline{M}} (C_C + C_T) + \tilde{K}_{\overline{D}} (C_{CC} + C_{CT} + C_{TT})\right)^{-1}$

The parameters, grouped into independent parameters, together with their literature values where available, are presented in Table 3.3. Because in Chapter 2 a first-order behavior in hydrogen for pressures $P_{H_2} \leq 0.6$ MPa was found, in line with Marangozis et al. (1977), Gut et al. (1979), and Stenberg and Schöön (1985), the kinetic rate constants were lumped with the hydrogen adsorption constant. However, strong deviations from first-order hydrogen dependency have been reported at pressures of P_{H_2} = 1.0–11.0 MPa, (Wisniak and Albright, 1961). Since the experimental pressure range in this chapter is larger than in Chapter 2, $K_{\overline{H}_2}$ can be

determined explicitly, considering that the linear behavior at $P_{H_2} \leq 0.6$ MPa turns into nonlinear Langmuir hydrogen adsorption at $P_{H_2} > 0.6$ MPa.

Table 3.3. Constants in the Diene Model

parameter	defined as	fitted value at T_{ref} = 393 K	E_a kJ/mol	source
$k_1 K_{\overline{H}_2}$ [a]	$k^{h}_{f,C} K_{H_2}$	4.14 [b]	32.2	from Chapter 2
$k_2 K_{\overline{H}_2}$ [a]	$k^{iso} / k^{h}_{f,i}$	1.53 [b]	47.2	from Chapter 2
$k_3 K_{\overline{H}_2}$ [a]	$k^{h}_{f,\overline{T}} / k^{h}_{f,\overline{C}}$	3.93 [b]	28.1	from Chapter 2
K_{iso}	$k^{iso}_{f,\overline{C}} / k^{iso}_{f,\overline{T}}$	3.5 [c]	-4.0 [d]	literature
$\tilde{K}_{\overline{M}}$	$K_{\overline{M}} / K_{\overline{S}}$	3.13 [e]	0	from Chapter 2
$\tilde{K}_{\overline{D}}$	$K_{\overline{D}} / K_{\overline{S}}$	[f]	[f]	this chapter
$K_{\overline{H}_2}$	eq 3.15	[f]	[f]	this chapter

[a] valid at $P_{H_2} \leq 0.6$ MPa only, where $q_{\overline{H}} \approx K_{\overline{H}_2} P_{H_2}$. [b] units: $kg_l / kg_{Ni} MPa\ s$. [c] Litchfield et al., 1963. [d] ΔH, Rogers et al., 1977. [e] dimensionless. [f] parameters determined in this chapter, Table 3.5.

A Runge–Kutta method with adaptive step size control (Press et al., 1989) was applied to integrate the rate equations for given parameter values. The parameters were optimized by the Levenberg–Marquardt method (Press et al., 1989) to obtain the minimal c^2, defined as

$$c^2 = \frac{1}{N_e} \sum \frac{1}{N_{e,d} N_{e,i}} \sum_{i=1}^{N_{e,i}} \sum_{d=1}^{N_{e,d}} \frac{(C^{e}_{e,i,d} - C^{m}_{e,i,d})^2}{s^2_{i,d}} \qquad (3.17)$$

Further, the procedure of chapter 2 was applied for avoiding intraparticle mass–transfer limitation (section 2.2.3). Also, the experiments were performed at such catalyst loads that the criterion for negligible gas-liquid mass transfer resistance was satisfied (see section 2.3 of Chapter 2).

3.3. Experimental Section

Hydrogenation experiments were performed in a well stirred semi-batch reactor of 380 mL (see Figure 3.3). The reactor was equipped with a gas inducing hollow axis stirrer, rotating at the maximum speed of 33 rps, four vertical baffles, electrical heating at the outer wall and an air cooling coil inside the vessel wall. The reactor temperature was controlled within 1 K and the pressure within 0.02 MPa.

The catalyst particles were regenerated in situ in a slurry of 90 g isopropyl myristate (IPM), a saturated fatty acid ester, at P_{H_2} = 0.5 MPa and T = 473 K for 2 h. It has been verified that maximum activity was achieved after this period. Possible solvent effects of IPM were not observed After evacuation and cooling, the reactor was put on pressure and the liquid reactant was added to the reactor from a pre-heated storage vessel by excess hydrogen pressure. Hydrogen was supplied from a pressurized bottle and monitored by a data acquisition system.

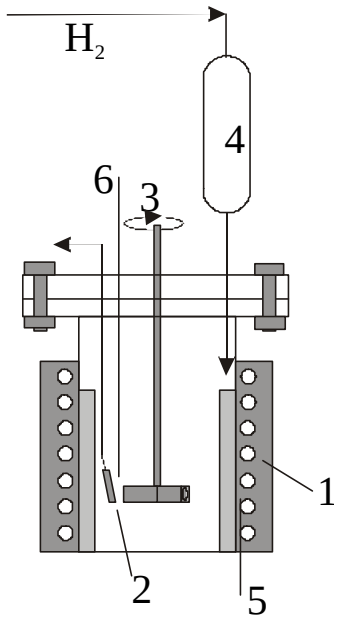

Figure 3.3. Experimental setup. 1, autoclave with external electrical heating; 2, sintered steel filter (1 *m*m) for liquid sampling; 3, stirrer; 4, hydrogen supply; 5, cooling coil in the wall; 6, temperature controller.

At equal conversion intervals, liquid samples were taken by removing 2 g of liquid from the reactor via a micro filter. The last V=10 mL of this sample liquid was isolated and diluted (1 %) in heptane. The amount of liquid present in the reactor after all samplings was recorded for correction of the catalyst load in the model calculations. The composition was determined by gas-liquid chromatography. The relative standard deviation for the combination of sampling and analysis ranged from 10 % at $x_i \approx 0.001$ to 0.5 % at $x_i \approx 1$.

Two different types of kinetic experiments were performed

a. Constant Hydrogen Pressure. In this type of experiments, batches of typically 90 g of sunflower methyl ester (SFME) were hydrogenated at constant T ($323 \leq T \leq 363$ K) and pressure ($0.3 \leq P_{H_2} \leq 3.5$ MPa). The consumption of hydrogen was calculated from the pressure decrease in the supply system. The fractions CC, CT, TC, TT, C, T, S, and IPM of 10–17 samples, taken during the reaction, gave the product distribution with time. A typical reaction profile is shown in Figure 3.8A.

b. Varying Hydrogen Pressure. These experiments were carried out at a constant temperature ($323 \leq T \leq 363$ K), but now the supply of hydrogen was stopped. The reactor pressure decreased due to hydrogen consumption from the head-space. A typical reactor pressure transient is shown in Figure 3.4. When the initial pressure was

P_{H_2} > 1 MPa, dP_{H_2}/dt was measured during successive periods of 40 seconds, where in between the pressure was extra reduced in a controlled way by opening a valve shortly. This way, rate data over the entire pressure range were obtained while keeping the liquid conversion low (z_{CC} < 0.1). A typical reactor pressure profiles of this type of experiment is shown in Figure 3.4.

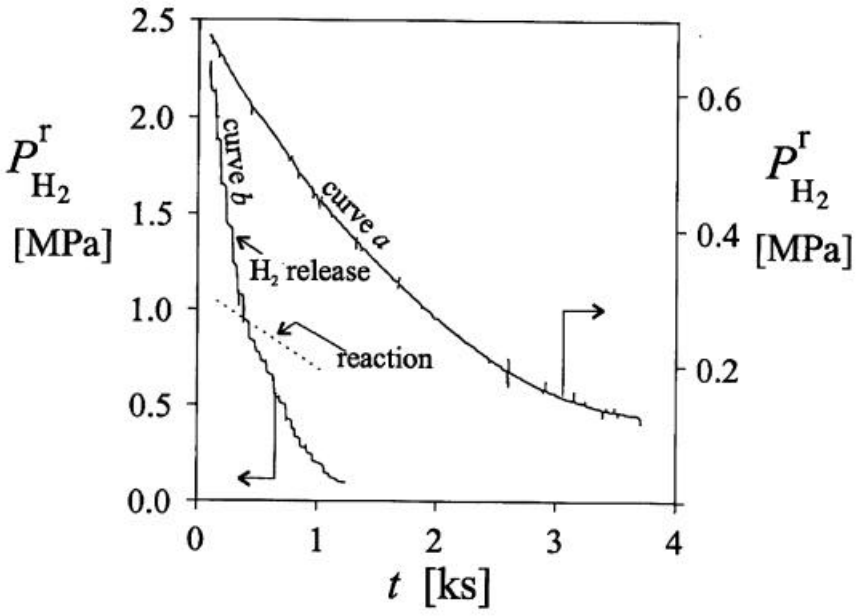

Figure 3.4. Reactor pressure transients of typical variable pressure experiments at T = 343 K. Line *a*, started at low pressure; line *b*, started at high pressure; dotted line, tangent, representing reaction rate.

The catalyst applied was Pricat 9910 (Unichema Emmerich, Germany). Properties of the catalyst particles can be found in the experimental section of Chapter 2. IPM and SFME were supplied by Unilever Research (Vlaardingen, The Netherlands) and SSOG (Milan, Italy). The IPM obtained was further purified with active Raney nickel at T = 473 K, P_{H_2} = 0.5 MPa, followed by filtering of the Raney-nickel. SFME was stirred with silica gel and molar sieves for 2 h under vacuum at T = 393 K to remove water and free fatty acids and filtered subsequently. The compositions after pretreatment are shown in Table 3.4.

3.4. Results

The gas–liquid volumetric mass-transfer coefficient was measured in hydrogenation experiments at high (12 kg_c/m^3_l) catalyst load (Stenberg and Schöön,

1985) yielding $k_l a$ = 0.8 s^{-1}. By adjusting the catalyst load, the gas–liquid hydrogen mass transfer resistance was kept below 10 % of the total resistance.

Table 3.4: Composition of SFME and IPM [a]

	SFME	IPM	
IPM		99.5	%
C16:0	6.9	0.3	%
C18:0	5.6		%
C18:1 *cis*-9	21.1		%
C18:2 *cis*,*cis*-9,12	64.6		%
C18:3 *cis*,*cis*,*cis*-9,12,15	0.1		%
C20:0	0.3		%
C22:0	0.8		%
C24:0	0.1		%
total phosphor	< 1	< 2	ppm
total sulphur	< 1	< 2	ppm
free fatty acid	0.09	0.12	%

[a] IPM = isopropyl myristate; SFME = sunflower methyl ester

3.4.1. Diene adsorption constant. Similarly to Chapter 2, the rate equations were first evaluated in the conversion domain instead of the time domain. In the conversion domain, i.e., the mole fractions of the fatty acids plotted as a function of the double bond conversion, the effects of *cis–trans* isomerization and diene-monoene selectivity on the component curves are pronounced, while nonmechanistic rate effects, such as catalyst activity variations and poisoning effects, are excluded. Further, the number of fit parameters is lower in this domain.

The ratio of double bond concentration over fatty acid concentration, x_{DB} is calculated from the mole fractions of monoenes and dienes according to

$$x_{DB} = x_C + x_T + 2(x_{CC} + x_{CT} + x_{TT}) \tag{3.18}$$

x_i is the mole fraction of i in the bulk liquid phase (C_i/C_{tot}). To get each experiment in a uniform conversion scale, the actual conversion is scaled to 100% L, which is equal to $x_{DB} \equiv 2$. The double bond conversion is than defined as

$$z_{DB} \equiv \frac{2 - x_{DB}}{2} \tag{3.19}$$

Substitution of eq 3.18 in eq 3.19 gives the double bond conversion as a function of the actual mole fractions

$$z_{DB} = 1 - \tfrac{1}{2}(x_C + x_T + 2(x_{CC} + x_{CT} + x_{TT})) \qquad (3.20)$$

Because of the use of a saturated compound as a solvent, the experiments usually start around z^0_{DB} = 0.5. The rate equations in the conversion domain are derived accordingly

$$R_i^c = \frac{R_i}{R_{DB}} = \frac{R_i}{R_C + R_T + 2(R_{CC} + R_{CT} + R_{TT})} \qquad (3.21)$$

By substitution of the time domain rate equations from Table 3.2 in eq 3.21, both the influences of hydrogen pressure, q_H and the catalyst activity, represented by k_1 (see also Chapter 2), are excluded from the conversion domain rate equations. By using the parameters for hydrogenation, isomerization and adsorption of the monoenes as determined in Chapter 2, only two parameters describe diene adsorption, $K_{D,ref}$ and ΔH_D.

In the reaction scheme, diene adsorption is uncoupled from *cis–trans* isomerization and therefore the analysis of the optimization results can be restricted to

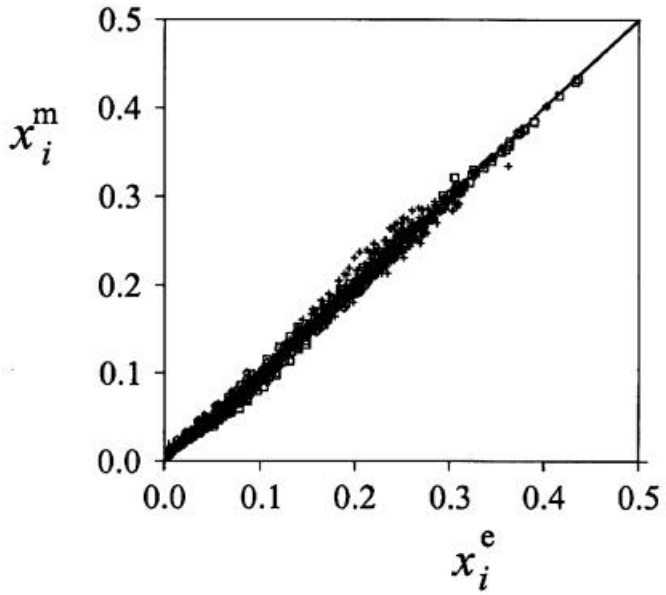

Figure 3.5. Parity plot of modeled versus experimental mole fractions after optimization of K_D^{ref} and ΔH_D to the set of constant pressure experiments in the conversion domain. G, dienes; +, monoenes; □, saturated. Experimental domain: 323 ≤ T ≤ 363 K and 0.4 ≤ P_{H_2} ≤ 3.5 MPa.

the groups of dienes, monoenes and saturated methyl ester only. The $K_{D,ref}$ and ΔH_D

were optimized for the complete set of constant pressure experiments simultaneously. The complete data set is shown in Figure 3.5. From Figure 3.5 it follows that the monoene concentrations are slightly underestimated, which is compensated for by the dienes and the saturated component. However, these deviations are small, so after

Table 3.5 Results of Stepwize Optimization of Unknown Model Parameters [a]

	first step	second step	final step	
domain:	conversion	time		units
parameter	constant pressure	variable pressure	constant and variable pressure	
$k_{1,ref}$		*(3.9± 1.0) x 10²*	*(3.6 ± 0.1) x 10²*	$kg_l/(kg_{Ni}\ s)$
$E_{a,1}$		*73.6 ± 4.8*	*66.1 ± 0.4*	kJ/mol
$\tilde{K}_{\bar{D},ref}$	*18.3 ± 0.3*	18.3	*22.7 ± 0.6*	
ΔH_D	*10.3 ± 0.3*	10.3	*12.9 ± 0.5*	kJ/mol
$K_{\bar{H}_2,ref}$		*0.065 ± 0.026*	*0.043 ± 0.002*	1/MPa
ΔH_{H_2}		*-53.8 ± 8.1*	*-50.3 ± 0.5*	kJ/mol

[a] see Table 3.3, $323 \le T \le 363$ K; $0.3 \le P_{H_2} \le 3.5$ MPa. Including 95% confidence boundary limits

optimization of only two fit parameters ($\tilde{K}_{\bar{D},ref}$ and ΔH_D) the model curves of monoenes and dienes show a remarkable agreement with the experimental data points for the whole set of data.

The initial parameter values were set at $\tilde{K}_{\bar{D},ref}$ = 3.13 (equal to monoene) and ΔH_D = 1 kJ/mol (a symbolic non-zero value). Different initial values resulted in the same optimal parameter values. The fitted values, presented in Table 3.5 under 'first step', result in diene adsorption constants of $9.2 \le \tilde{K}_{\bar{D}} \le 18.3$ at $323 \le T \le 393$ K. Since $\tilde{K}_{\bar{D}}$ denotes the ratio of diene over saturated adsorption, these values show that preferent adsorption of the double bonds relative to the adsorption of saturated fatty acid methyl esters increases with temperature and, because $\tilde{K}_{\bar{M}}$ is constant, so does the preferential adsorption of diene over monoene.

3.4.2. Hydrogen Adsorption Constant. The variable hydrogen pressure experiments were performed to elucidate the influence of the hydrogen pressure on the conversion rate. Because of the linear dependency of R_i on q_H, K_H can directly be obtained from these experiments (see Table 3.2). In all these experiments, the initial concentrations of unsaturated compounds were the same and the maximum conversion of the fastest reactant, i.e., methyl linoleate, was always below 10 % and thus

negligible. The concentrations of the liquid components can therefore be considered constant in these experiments and the rate equations of Table 3.2 reduce to pseudo first-order expressions with respect to the hydrogen surface coverage

$$\frac{R_i}{m_c} = -k_i^{'} q_H = -k_i^{'} \frac{K_{H_2} P_{H_2}}{1 + K_{H_2} P_{H_2}} \qquad i = \mathrm{CC, CT, TT, C, T} \qquad (3.22)$$

The hydrogen reaction rate is calculated from:

$$R_{H_2} = 2(R_{CC} + R_{CT} + R_{TT}) + R_C + R_T = m_c k_{H_2}^{'} \frac{K_{H_2} P_{H_2}}{1 + K_{H_2} P_{H_2}} \qquad (3.23)$$

Because of the equimolar stoichiometry of the reaction, R_{H_2} is equal to the double bond conversion rate, R_{DB}, and therefore represents the overall hydrogenation rate. This hydrogenation rate in the liquid phase is calculated from the hydrogen pressure drop in the reactor via the mass balance:

$$f_{H_2} = R_{H_2} V_l = 10^6 \frac{dP_{H_2}^r}{dt} \frac{V_r (e_G + m_{H_2}(1 - e_G))}{RT} \qquad (3.24)$$

Eq 3.24 accounts for the decrease in dissolved hydrogen with decreasing pressure, which proved to be significant in the applied pressure ranges. The pseudo first-order rate constant, $k_{H_2}^{'}$, can be calculated from the actual composition and the values of the parameters k_2, k_3, K_{iso}, $\tilde{K}_{\overline{M}}$ from Table 3.3 and $\tilde{K}_{\overline{D},ref}$ and DH_D from Table 3.6. The remaining model parameters $K_{\overline{H}_2,ref}$ and DH_{H_2} can then be fitted such that c^2 of eq 3.17 is minimal for the complete set of variable pressure experiments (N_e=12). The lumped value of $k_1 K_{\overline{H}_2}$ of Chapter 2 (Table 3.3) is not applicable here, because it was determined in the pressure range $0.02 \leq P_{H_2} \leq 0.50$ MPa at $T \geq 353$ K where the hydrogenation rate is linear with hydrogen pressure. In contrast, it is known from literature data on adsorption enthalpies (Susu and Ogunye, 1981; Konvalinka et al., 1981) that at the low temperatures of $T < 353$ K, $K_{\overline{H}_2} P_{H_2}$ is not negligible in the denominator of eq 3.13 at pressures of $P_{H_2} \leq 0.5$ MPa. Therefore, $k_{1,ref}$ and $E_{a,1}$ were fitted simultaneously, which gave a close agreement with the experimental points (see Figure 3.6).

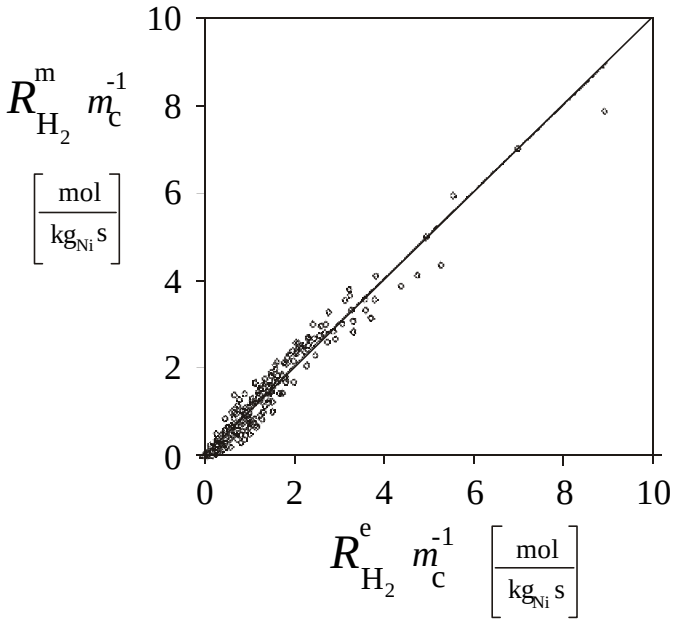

Figure 3.6. Parity plot of the modeled versus the experimental hydrogen reaction rates after optimization of K_{H2}^{ref} and DH_{H2} to the variable hydrogen pressure experiments. Experimental domain: $0 \leq P_{H_2} \leq 3.2$ MPa and $323 \leq T \leq 363$ K.

The fitted value for DH_{H_2}, see Table 3.5, is in agreement with literature data obtained from H_2/D_2 exchange experiments (DH_{H_2} = –51.3 kJ/mol; Niklasson et al., 1987) and temperature programmed desorption experiments at high coverages (i.e., more than a mono layer): for instance, Konvalinka et al. (1981) found DH_{H_2} = –48 to –71 kJ/mol on Ni catalysts. At lower occupancies $q_{\overline{H}} < 0.1$, they found the adsorption enthalpy to rise to DH_{H_2} = –130 kJ/mol. Under hydrogenation reaction conditions, Susu and Ogunye (1981) found DH_{H_2} = –52.3 kJ/mol, while Gut et al. (1979) found a completely different value, DH_{H_2} = +1.3 kJ/mol. The latter can be due to their narrow experimental pressure range ($0.22 \leq P_{H_2} \leq 0.34$ MPa), which results in minor pressure related variations in the data set only, and, therefore, low reliability of the fitted hydrogen adsorption parameters. The hydrogen surface occupancies calculated from Gut et al. (1979), Susu and Ogunye (1981), and the present work are shown in Figure 3.7 together with the pressure ranges applied. The results of Susu and Ogunye (1981) predict an approximately constant $q_{\overline{H}}$ for P_{H_2} > 1 MPa, which implies a constant hydrogenation reactivity. This is in contradiction with the experimental data of Wisniak and Albright (1961), who found an increasing hydrogenation rate with pressure up to P_{H_2} = 10 MPa, and with the results of this work, see Figure 3.7.

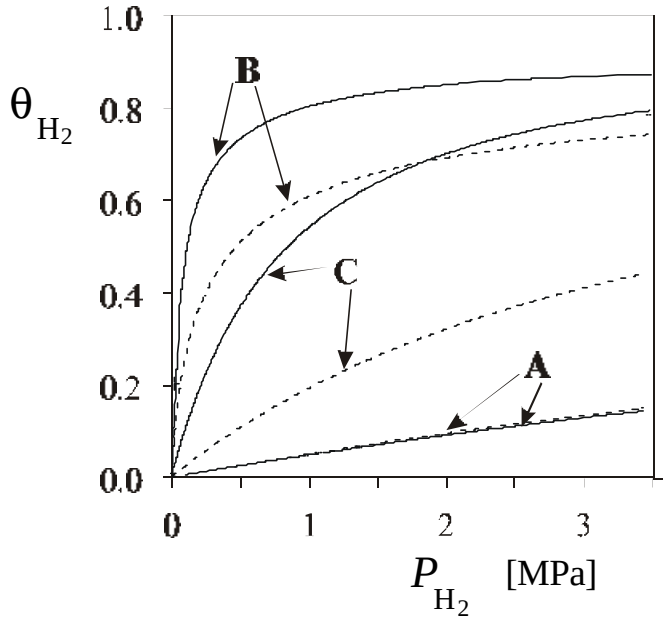

Figure 3.7. Modeled surface occupancies of hydrogen as a function of pressure. The hydrogen adsorption parameters were determined from fits of Langmuir-type kinetic models to hydrogenation experiments. 323 K; – – – - 353 K; **A**, Gut et al. (1979), determined at 0.22 ≤ P_{H_2} ≤ 0.34 MPa and 411 ≤ T ≤ 511 K; **B**, Susu and Ogunye (1981), determined at 0.37 ≤ P_{H_2} ≤ 0.65 MPa and 393 ≤ T ≤ 453 K; **C**, present work, determined at 0.3 ≤ P_{H_2} ≤ 3.5 MPa and 323 ≤ T ≤ 363 K.

3.4.3. Final Optimization. In the time domain, a simultaneous optimization of $\dot{K}_{\overline{D},ref}$, DH_D, $K_{\overline{H}_2,ref}$, $k_{1,ref}$, and $E_{a,1}$ was performed to the combined sets of constant and variable hydrogen pressure experiments. In Table 3.5 the column denoted “final step” represents the optimized values, fitted on all experiments simultaneously. The start values of the parameters for the optimization are taken from (the conversion domain) constant hydrogen pressure fit and the variable hydrogen pressure fit. The minor adjustment of the parameters justifies the use of both types of data ranges for a preliminary optimization of the parameters.

The model curves of the "dienes" (sum of diene isomers), "monoenes" and saturates are in good agreement with the experimental data, see Figure 3.8. The strong adsorption of the dienes relative to the monoenes, introduces a selective hydrogenation of diene over monoene. The deviations of the fit of the model to the total data set in the time domain, presented in Figure 3.9, are below 10% for the constant pressure experiments. The remaining deviation is mainly caused by variations in catalyst activity in the various batch experiments.

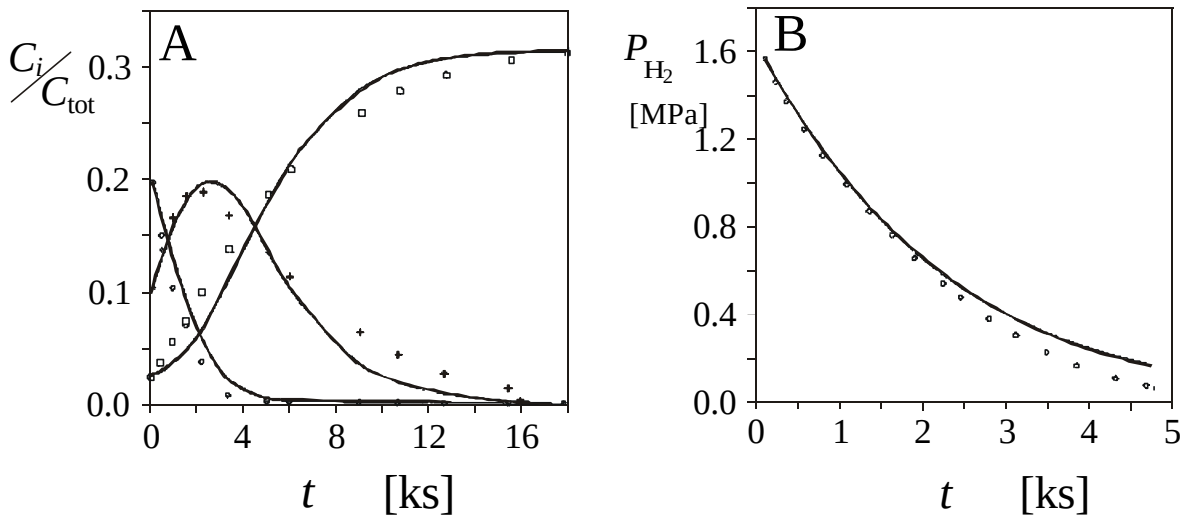

Figure 3.8. Model curves after the final optimization (see Table 3.6). **A**, A typical constant pressure experiment, T = 353 K, P_{H_2} = 2.0 MPa, m_c = 7.1 × 10^{-2} kg_{Ni}/m_l^3; G, dienes; +, monoenes; □, saturated; **B**, A typical variable pressure experiment, T = 343 K and m_c = 7.4 × 10^{-2} kg_{Ni}/m_l^3; circles are experimental points.

In the isomers curves, Figure 3.10, the fits of CC, C, T, and S are remarkably good

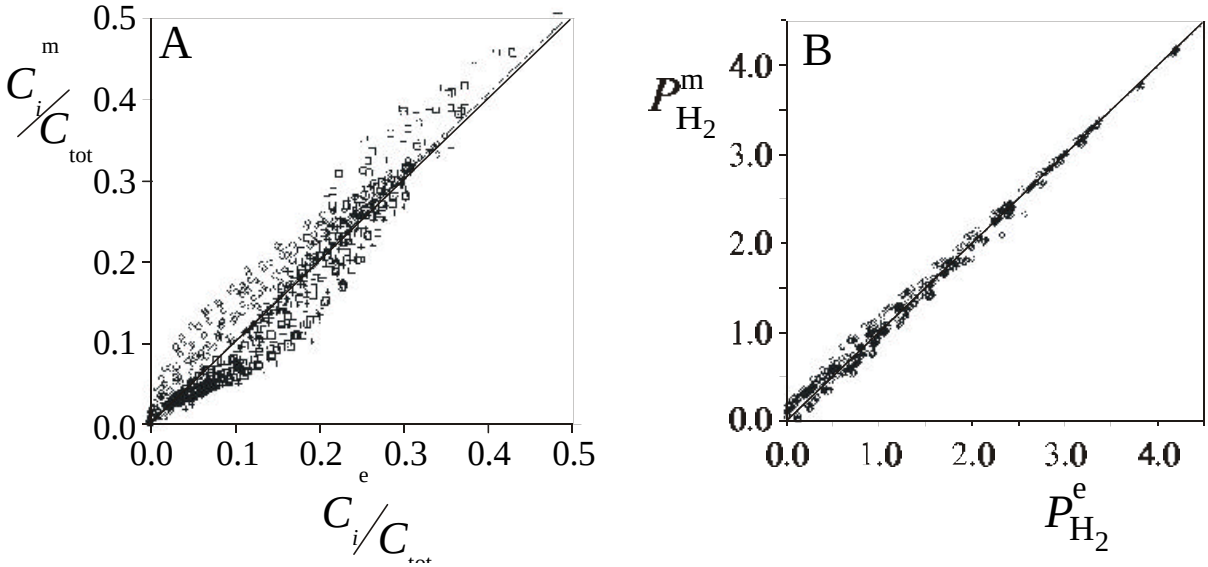

Figure 3.9. Parity plots of the modeled versus the experimental data points after the final optimization. **A**, constant pressure experiments; G, dienes; +, monoenes; □, saturated; **B**, variable pressure experiments.

if one considers that none of the fitted parameters had effect on *cis–trans* isomerization. It can therefore be concluded that the *cis–trans* isomerization parameters, as obtained for monoene hydrogention in Chapter 2, are indeed applicable to diene hydrogenation as well.

Figure 3.11 compares the selectivity of the hydrogenation of diene relative to monoene, predicted by the present kinetic model with the available literature data. For this purpose it is customary to consider the rate equations of the scheme $\mathrm{D} \xrightarrow{k'_{\mathrm{D}}} \mathrm{M} \xrightarrow{k'_{\mathrm{M}}} \mathrm{S}$ as first order ($R_{\mathrm{D}} = m_{\mathrm{c}} k'_{\mathrm{D}} C_{\mathrm{D}}$, $R_{\mathrm{M}} = m_{\mathrm{c}} k'_{\mathrm{M}} C_{\mathrm{M}}$) so that the selectivity S_{I} defined as (Veldsink et al., 1997):

$$S_{\mathrm{I}} = \frac{k'_{\mathrm{D}}}{k'_{\mathrm{M}}} \tag{3.28}$$

The rate equations in Table 3.2 reduce to first order kinetics for $C_{\mathrm{S}}/C_{\mathrm{tot}} \rightarrow 1$, because then $(C_{\mathrm{S}} / C_{\mathrm{tot}}) >> \tilde{K}_{\overline{\mathrm{M}}} (C_{\mathrm{M}} / C_{\mathrm{tot}}) + \tilde{K}_{\overline{\mathrm{D}}} (C_{\mathrm{D}} / C_{\mathrm{tot}})$ in the denominator of

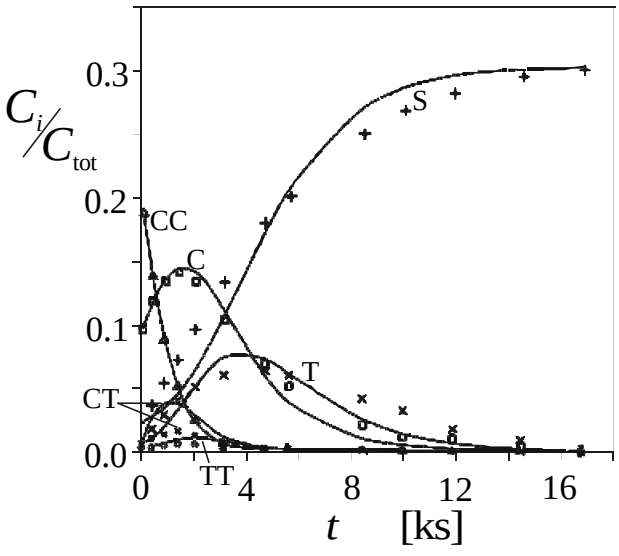

Figure 3.10. Mole fractions of all components for the experiments in Figure 3.8. Δ, CC (*cis-cis*); ❋, CT (*cis-trans* and *trans-cis*); G, TT (*trans-trans*); ×, T; ð, C; +, S.

those rate equations. Following the definition of the selectivity, eq 3.28, the linoleate over oleate hydrogenation selectivity consequently reads

$$S_{\mathrm{I}} = \frac{\tilde{K}_{\mathrm{D}}}{\tilde{K}_{\mathrm{M}}} \qquad (3.29)$$

Since the rate equations in Table 3.2 exhibit equal pressure dependency, eq 3.29 is independent of the hydrogen pressure. Our selectivities, obtained in the pressure range $0.2 \leq P_{\mathrm{H_2}} \leq 3.5$ MPa correspond nicely with the data of Albright and Wisniak (1962) which were determined at $P_{\mathrm{H_2}} > 1.0$ MPa, and Pihl and Schöön (1971), who accounted for a power law influence of hydrogen in the selectivity calculations. At pressures $P_{\mathrm{H_2}} < 0.5$ MPa, where the experiments of Gut et al. (1979) and Ray and Carr (1985) were performed, selectivity is known to increase strongly with decreasing pressure (see Veldsink et al. 1997 for a discussion of these data). The influence of the hydrogen pressure on the selectivity is believed to be caused by conjugation of the double bonds in the dienes, which is enhanced at low availability of hydrogen at the catalyst surface (Coenen, 1960). This subject, however, will be addressed in more detail in a follow-up study.

The agreement of the present model with literature data is further emphasized by our predictions on the cottonseed oil hydrogenation data of both Eldib and Albright (1957), which are known to be free of mass transfer limitations (Marangozis et al., 1977), and Pihl and Schöön (1971), who performed extensive testing to exclude mass transfer limitations. The results in Figure 3.12 were obtained by using their experimental values for T, $P_{\mathrm{H_2}}$, and the initial mol fractions, x_{i}^0 input only.

3.5. Conclusions.

Kinetic rate expressions which were developed for the hydrogenation of double unsaturated fatty acid methyl esters and are based on an extension of the model for hydrogenation of mono unsaturated methyl esters of Chapter 2 appear to be capable of accurately describing the observed diene selectivity and the monoene (*cis–trans*) isomers transients in diene hydrogenations at the conditions tested ($324 \leq T \leq 363$ K and $0.3 \leq P_{\mathrm{H_2}} \leq 3.5$ MPa), provided the preferential adsorption of dienes relative to monoenes are taken into account. Due to the larger experimental pressure range in the hydrogenation experiments compared to Chapter 2, it was necessary to determine the hydrogen adsorption parameters separately from the kinetic constants.

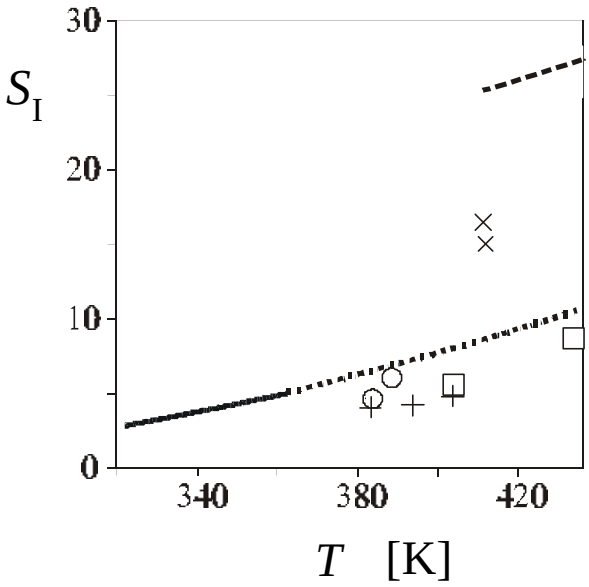

Figure 3.11. Selectivity S_I as a function of temperature. ○ 1.0 MPa, + 2.0 MPa, Albright and Wisniak (1962); □ 0.05–0.1 MPa, Pihl and Sch¬¬n (1971); × 0.39 MPa, Ray and Carr (1985); - - - 0.22–0.34 MPa, Gut et al. (1979); 0.3-3.5 MPa, this work; Λ this work extrapolated.

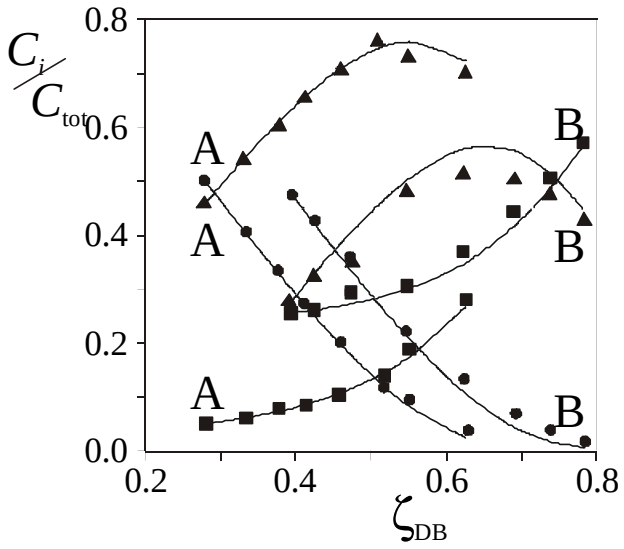

Figure 3.12. Model predictions of cottonseed oil hydrogenation data of **A**, Pihl and Sch¬¬n (1971), T = 433 K, P_{H_2} = 0.11 MPa; **B**, Eldib and Albright (1957), T = 403 K, P_{H_2} = 0.41 MPa. ●, dienes; s, monoenes; n, saturated.